Journal of Liposome Research

ISSN: 0898-2104 (Print) 1532-2394 (Online) Journal homepage: www.tandfonline.com/journals/ilpr20

Pyrophosphate-modified liposomes for bone-targeted delivery

Alberto Dal Corso, Riccardo Becchetti, Cristina Matteo, Sara Turchetti, Paola Fabbrizio, Marta Cancelliere, Gaia Ghiselli, Marina Meroni, Giovanni Nardo, Massimo Zucchetti, Roberta Frapolli & Claudia Nastasi

To cite this article: Alberto Dal Corso, Riccardo Becchetti, Cristina Matteo, Sara Turchetti, Paola Fabbrizio, Marta Cancelliere, Gaia Ghiselli, Marina Meroni, Giovanni Nardo, Massimo Zucchetti, Roberta Frapolli & Claudia Nastasi (28 Dec 2025): Pyrophosphate-modified liposomes for bone-targeted delivery, Journal of Liposome Research, DOI: 10.1080/08982104.2025.2599839

To link to this article: https://doi.org/10.1080/08982104.2025.2599839

JOURNAL OF LIPOSOME RESEARCH
https://doi.org/10.1080/08982104.2025.2599839

Taylor & Francis
Taylor & Francis Group

RESEARCH ARTICLE

OPEN ACCESS Check for updates

Pyrophosphate-modified liposomes for bone-targeted delivery

Alberto Dal Corso[a], Riccardo Becchetti[b], Cristina Matteo[b], Sara Turchetti[b], Paola Fabbrizio[c], Marta Cancelliere[b], Gaia Ghiselli[b], Marina Meroni[b], Giovanni Nardo[c], Massimo Zucchetti[b], Roberta Frapolli[b] and Claudia Nastasi[b]

[a]Department of Chemistry, Università degli studi di Milano, Milan, Italy; [b]Department of Experimental Oncology, Laboratory of Cancer Pharmacology, Istituto di ricerche farmacologiche Mario Negri (IRCCS), Milan, Italy; [c]Department of Neuroscience, Laboratory of Molecular Neurobiology, Istituto di ricerche farmacologiche Mario Negri (IRCCS), Milan, Italy

ABSTRACT

Bone-related diseases and bone cancers remain challenging to treat due to limited targeted therapies and significant off-target side effects. This study presents the development of a bone-targeted liposomal formulation, termed Bone Binding Liposomes (BBL), functionalized with a pyrophosphate-cholesterol derivative to enhance binding to bone mineral (hydroxyapatite). Our experiments demonstrated the superior affinity of BBL compared to conventional Non-Binding Liposomes (NBL). Moreover, both formulations efficiently encapsulated a prototype drug and both exhibited comparable biocompatibility, both preserving the drug's physicochemical properties on elective target cells, macrophages. This targeted delivery system holds a potential for treating bone-related diseases, offering a means to improve targeted delivery and reduce off-target effects.

ARTICLE HISTORY
Received 29 July 2025
Revised 14 October 2025
Accepted 1 December 2025

KEYWORDS
Liposomes; bone; targeted therapy; macrophages; resiquimod

Introduction

Bones play a crucial role in providing support and stability to the body, creating a structural framework that supports muscles, organs, and tissues, enabling functional motion and protecting against external impacts. Bone tissue is continuously remodeled, growing, and repairing itself in response to factors like mechanical stress, hormonal fluctuations, and metabolic needs [1–3]. This ongoing process allows bones to adjust to the body's evolving demands during growth, physical activity, injury, or illness, through the modulation of mineral balance, particularly calcium homeostasis [2]. Bone diseases cover a broad spectrum of conditions that impair the skeletal system, weakening bone structure, strength, and overall health. Common disorders include osteoporosis, rheumatoid arthritis, Paget's disease, osteogenesis imperfecta, osteonecrosis, fibrous dysplasia, rickets, and osteomyelitis [4].

Another significant category is bone cancers, such as osteosarcoma and Ewing sarcoma, which currently lack effective, targeted therapies [5,6]. Moreover, other types of primary cancers can spread to the bones causing metastasis, leading to pain, bone weakening, and fractures [7–9]. Bone is one of the most common sites of metastasis from advanced solid cancers. Bone metastases occur in 65–80% of patients with advanced prostate or breast cancer, 40–50% patients with lung cancer and in <10% of those with gastrointestinal cancer [9]. Moreover, those typically have a poor prognosis and quality of life [10]. Therefore, there is an urgent clinical need to develop new and effective treatments also for bone metastatic cancers [4,8,9,11].

To enhance treatment outcomes, increase drug efficacy, and minimize side effects in bone disease management, bone-targeted nanomedicine and nano-delivery systems hold great promise [12,13] also for treating solid tumors [14,15]. Among all types of nanoparticles for drug delivery, liposomes are the most developed and well-established drug delivery system available clinically [16,17]. Liposomes are composed of phospholipidic and cholesterol building blocks making them biocompatible and allowing them to fuse with cell membranes and easily improve the cellular uptake of the encapsulated drug. The preparation procedure strongly affects the structures and size of liposomes; accordingly, they can be categorized into small, large, and giant unilamellar or multilamellar vesicles with diameters of 20–100 nm, 100–1000 nm, larger than 1000 nm, and more than 500 nm, respectively [18].

The unique ability of liposomes to encapsulate both lipophilic and hydrophilic compounds allows them to deliver drugs with different physicochemical properties. They provide several advantages such as biodegradability, low or absent immunogenicity, increased drug solubility, sustained drug release, increased drug concentration at the target site, overcoming multidrug resistance (MDR), and improving the therapeutic index [19]. Moreover, they offer several benefit over drug solutions, including reduced toxicity of the encapsulated drug [20], prolonged systemic circulation when surface-modified (e.g. PEGylated liposome), improved pharmacokinetics [21], controlled drug release kinetics [22], and tumor targeting [19]. For these reasons, they

CONTACT Claudia Nastasi claudia.nastasi@marionegri.it Department of Experimental Oncology, Laboratory of Cancer Pharmacology, Istituto di ricerche farmacologiche Mario Negri (IRCCS), Via Mario Negri 2, 20156 Milan, Italy.
Supplemental data for this article can be accessed online at https://doi.org/10.1080/08982104.2025.2599839.

have been largely studied in several studies to deliver different types of drugs from chemotherapy to antimicrobial, and many others [23,24].

However, despite demonstrating substantial drug accumulation in various pre-clinical and human tumors [25], clinically approved liposomal formulations like DoxilH/CaelyxH (pegylated liposomal doxorubicin) and MyocetH (un-pegylated liposomal doxorubicin) have only led to a modest improvement in anti-tumor efficacy compared to the standard treatments [26–28].

The functionalization of liposomes surfaces with specific small molecules, capable of selective binding to specific-associated antigens, offers a valuable opportunity to target the drug release at the disease site, although it is seriously challenging to achieve [29]. Bone-targeting drug delivery systems are of major importance because they allow selective accumulation of therapeutic agents at skeletal sites, thereby enhancing efficacy while minimizing systemic side effects.

The abundance of hydroxyapatite (HA), the main inorganic component of bone, provides a natural docking site for molecules with strong affinity to calcium phosphate crystals, such as bisphosphonates and pyrophosphate, that have been exploited to improve the accumulation of therapeutics to diseased bone tissues (from primary bone tumors or secondary metastases to rheumatoid arthritis, osteoporosis, etc.) [4,12,30]. For instance, bisphosphonates demonstrate strong and specific binding affinity to HA. By inhibiting osteoclasts activity, they offer an added therapeutic benefit that have been clinically validated for the treatment of bone resorption disorders [1,31].

This dual advantage—biological relevance and established safety—makes pyrophosphate-derived ligands powerful tools for designing next-generation bone-targeted drug delivery systems with applications in oncology, orthopedics, and regenerative medicine.

In this paper, we describe the synthesis and analysis of a classical liposome formulation (named non-binding liposomes, NBL) in comparison with a new bone-targeted liposomal formulation (named bone-binding liposomes, BBL), which carry pyrophosphate-cholesterol adducts. To characterize and compare NBL and BBL formulations we arbitrarily selected resiquimod (R848), as therapeutic payload; it is an imidazoquinoline drug, chosen to investigate drug release and efficacy tests *in vitro* upon immune cells.

R848 is in fact an agonist for Toll-like receptors 7 and 8 (TLR7/8), mostly expressed by various human and murine immune cells like dendritic cells, neutrophils, and particularly macrophages. It induces the expression of NF-κB-related genes via the TLR7/8 MyD88-dependent signaling pathway [32,33]. Macrophages are tissue-resident cells, generally classified into: (i) M0 which are naïve cells, in a steady state, (ii) M1 which are pro-inflammatory (and anti-tumoral when in the tumor microenvironment (TME)), and (iii) M2 which show a role in wound healing processes, and immunosuppressive profile when in the TME.

Due to the immunostimulatory effects, R848 have been exploited to induce M2 macrophages acquiring a M1-like phenotype, expressing proinflammatory markers and secreting chemokines and cytokines fundamental for the innate and adaptive immune system to fight tumor cells [34,35]. In particular, tumor-associated macrophages (TAMs) are highly abundant in several types of tumors and metastasis. In general, their presence is positively correlated with tumor progression, while a high prevalence of M2 subtype is linked with poor prognosis [36]. Thus, this targeting system could be exploited in the case of primary or secondary tumors that affect the bones or for non-oncologic diseases, by loading them with the proper disease-specific therapeutic.

Results and discussion

Synthesis and characterization of NBL and BBL

The hydroxy group of cholesterol was derivatized to install a hydrophilic triethylene glycol (PEG3) spacer and a pyrophosphate unit. Intermediates were purified by flash chromatography and characterized by nuclear magnetic resonance (NMR) and mass spectrometry. The final cholesterol-PEG3-pyrophosphate adduct was purified by dialysis. Liposomes were synthesized using DSPC and cholesterol (for NBL) or DSPC, cholesterol and PPi-PEG3-Cholesterol (for BBL) performing the film-hydration method, followed by extrusion with 200 and 100 nm polycarbonate filters (as described in Materials and methods). The effective hydrodynamic diameters, the polydispersity index (PDI), and the ζ-potential of the formulated liposomes were characterized by dynamic light scattering (DLS).

Firstly, we optimized the protocol to synthesized NBL and BBL. DLS analysis revealed comparable sizes (mean: 147 ± 17.2 vs 148 ± 18.9 nm), a ζ-potential more negative for BBL due to the negative charge of the pyrophosphate group (−5.5 ± 1.4 vs −15.5 ± 1), and similar PDI (0.1 ± 0.06 vs 0.1 ± 0.01) ($n = 4$).

BBL bind the bone matrix

To prove the BBL affinity for the hydroxyapatite, fluorescent-labeled (DiI) NBL and BBL were used. Murine bones were exposed to both formulations for 2h and 24h at 37 °C, and after several washing steps, pictures were acquired using confocal microscopy. The *in vitro* assay revealed signals primarily from fluorescent BBL that remain attached to the bone matrix, while low signal with the NBL did not support any binding (Figure 1(A–B)). Furthermore, the signal emitted by BBL increased over time, from 2h to 24h. These data confirm the superior binding affinity of the BBL formulation compared to the NBL one.

Synthesis of drug-loaded NBL and BBL

To study the liposomes loading efficiency, release kinetics and drug protection we then started to load both formulations with the chosen drug.

The effective hydrodynamic features of drug-loaded NBL and BBL were studied by DLS. The sizes of both were very similar (NBL 144.8 ± 13.7 vs BBL 148.8 ± 15.5 nm) (Figure 2(A)), different ζ-potential considering the (NBL −9 ± 4.24 vs BBL −28.7 ± 5) (Figure 2(B)) and almost equal PDI (NBL 0.07 ± 0.04 vs BBL 0.09 ± 0.04) (Figure 2(C)) ($n = 9$).

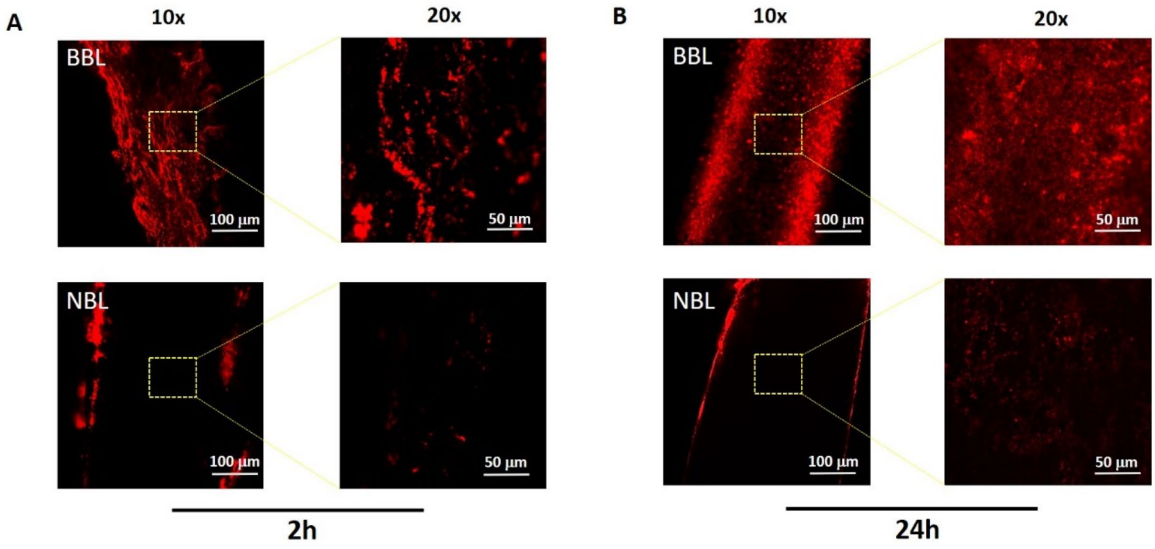

Figure 1. Confocal micrographs of ex vivo bones. Bones were incubated with fluorescent BBL or NBL for 2h or 24h and then washed 10 times with PBS to remove unbound liposomes before image acquisition. (A) 2h and (B) 24h exposure 10x and 20x magnification are displayed.

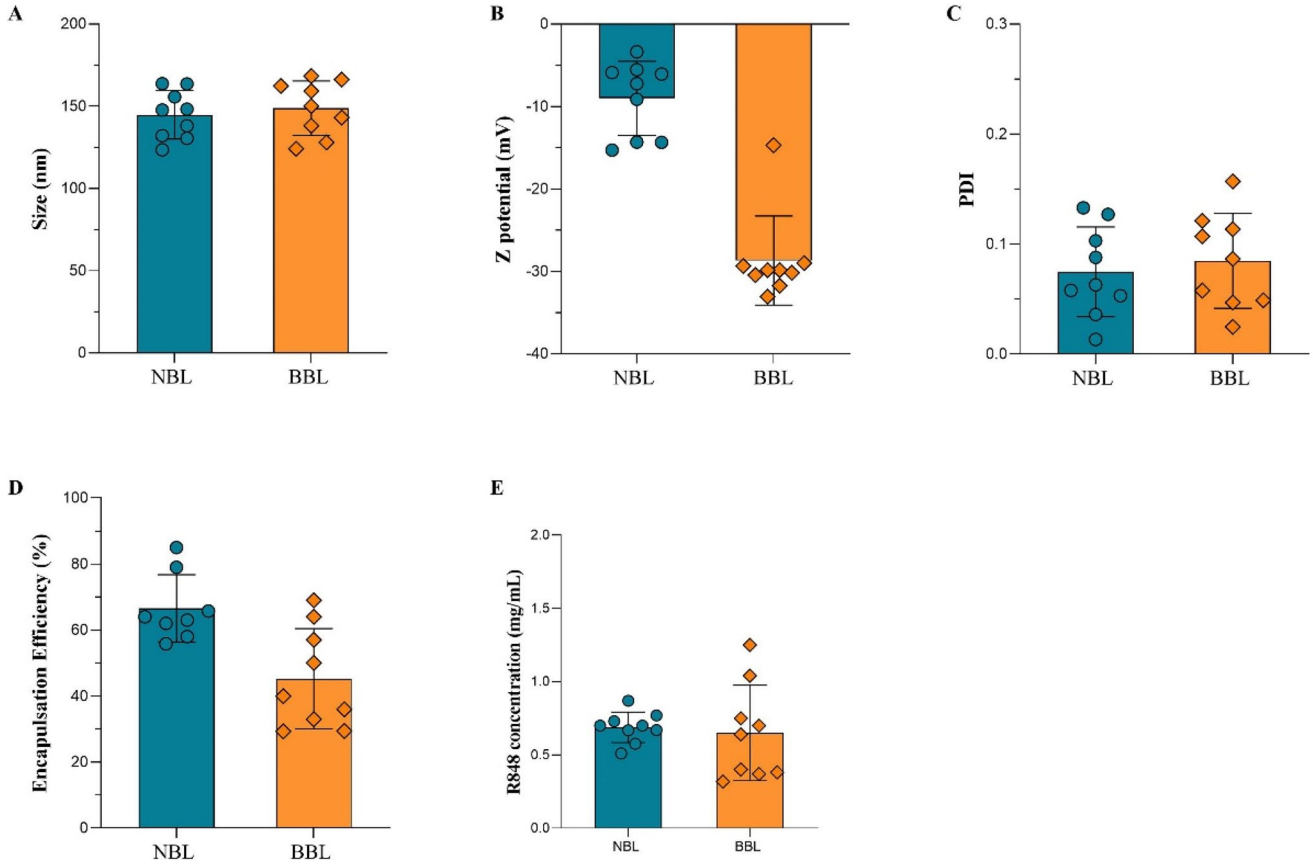

Figure 2. Characterization of drug-loaded NBL and BBL by DLS. Charts show (A) the size, (B) the z potential, (C)the PDI, (D)the encapsulation efficiency, (E) and the drug's loaded concentration. The chart's bars represent the mean ± SD, with dots representing single independent experiments (n = 9).

HPLC analysis indicated that the encapsulation efficiency (EE%: calculated as mg of drug used divided to mg of drug quantified by HPLC *100) of R848 was 68% ± 9 for the NBL and 45.30% ± 14.3 for the BBL (Figure 2(D)) with a loaded average concentration of 0.69 ± 0.1 mg/ml for NBL and 0.65 ± 0.3 mg/ml for BBL ($n = 9$) (Figure 2(E)).

Liposome in vitro kinetics release of the drug

BBL and NBL were separately loaded into dialysis cassettes of 3.5 KDa molecular weight cutoffs and left floating into a buffer mimicking physiological conditions (solution of 40% bovine albumin, 37 °C) to test the retention efficacy of those two formulations.

At several time points (0.08, 0.25, 0.50. 1, 2, 4h), the cassettes were taken off the buffer and aliquots were sampled for HPLC-UV quantification of the retained drug and then put back. The release kinetics showed similar trends, retaining about 75% of the loaded R848 within the first 2 h and about 50% of the drugs for both NBLs and BBLs at 4h (Figure 3). These *in vitro* data showed that both formulations show a comparable trend of drug release, confirming that the pyrophosphate-cholesterol in BBL did not compromise the liposome features and drug's release kinetics.

NBL and BBL are internalized by the same mechanisms

Liposomes are internalized by cells through various mechanisms including endocytosis (clathrin-mediated, caveolae-mediated) and macropinocytosis, and fusion with the cell membrane [37,38]. Classically, endocytosis can be divided into pinocytosis and phagocytosis. Pinocytosis involves internalization of fluid while phagocytosis, an actin-dependent process, involves internalization of large particles such as bacteria. Pinocytosis can be further divided into those that are dependent on the clathrin coat (clathrin-mediated endocytosis, CME) or those that are independent of clathrin (clathrin-independent endocytosis, CIE). To study the mechanism by which liposomes formulation are internalized, we inhibited the endocytosis, both CME and CIE, and the micropinocytosis via PitStop2, Filipin III, and amiloride, respectively [37]. PitStop2 interferes with binding of proteins to the N-terminal domain of clathrin, inhibiting CME; Filipin III Binds to cholesterol in the membrane, inhibiting CIE; EIPA amiloride Inhibits Na+/H + exchange, inhibiting micropinocytosis.

We analyzed over time the fluorescence emitted by the DiI labeled NBL and BBL after treatments. We observed that BBL were internalized slightly faster than NBL and, overall, both formulations are internalized by caveolin-dependent endocytosis and micropinocytosis since their specific block significantly inhibited the increase of the percentage of cells positive to fluorescent liposomes (Figure 4A–B).

A key aspect for successful drug delivery via lipid-based nanoparticles is their internalization in target cells. Our data showed that the chemical modification of cholesterol does not alter the internalization of BBL compared to NBL, allowing the release of the drug and its downstream effect, as shown in the next paragraphs.

BBL on murine macrophages: cytotoxicity, internalization kinetics, and expression markers

To check whether NBL and BBL were cytotoxic upon target cells, primary bone marrow-derived macrophages (BMDM)

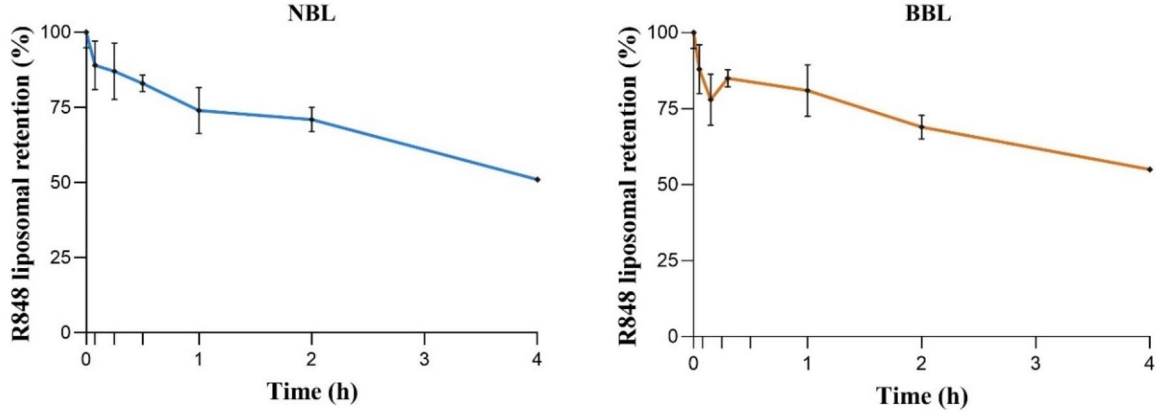

Figure 3. NBL and BBL in vitro release kinetics. NBL or BBL solutions were loaded into dialysis cassette of 3.5 KDa molecular weight cutoffs (MWCOs) in physiological conditions (40% albumin, 37 °C). The quantification of the retained drug was performed, and data were plotted as percentages relative to time zero (n = 3).

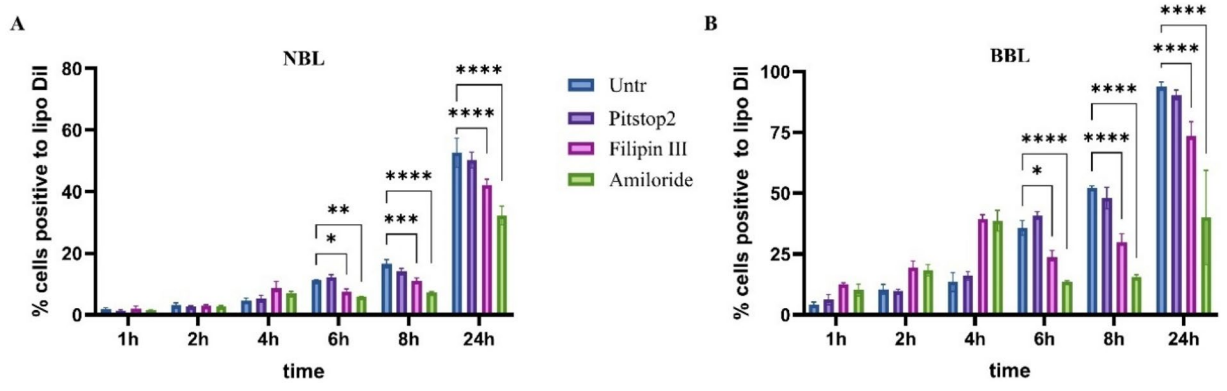

Figure 4. Inhibition of endocytosis and micropinocytosis clathrin- or claveolin-mediated endocytosis or micropinocytosis. Inhibition was followed over time with the use of specific blocking drug like Pitstop2 (25uM), Filipin III (0,5 µg/mL), EIPA amiloride (10 µg/mL). Statistically significant differences are expressed as follows: *$p < 0.05$; **$p < 0.01$; ***$p < 0.0001$; ****$p < 0.00001$.

were generated as the best candidate to test drug release and its effect upon target cells. M0 *naïve* cells were exposed to each loaded formulation or free drug up to 48h. The viability was measured using a viability marker for flow cytometry; the fluorescence emitted by dead cells was excluded, and live cells were quantified. Neither NBL nor BBL altered the cell's viability compared to control and free drug R848 (Figure 5(A)), confirming their safe profile.

Additionally, BBL were stained with lipophilic tracer DiI and used to study the internalization kinetics by its fluorescence emission. As shown by the increased geometric mean of fluorescence intensity (gMFI) in Figure 5(B), the liposome

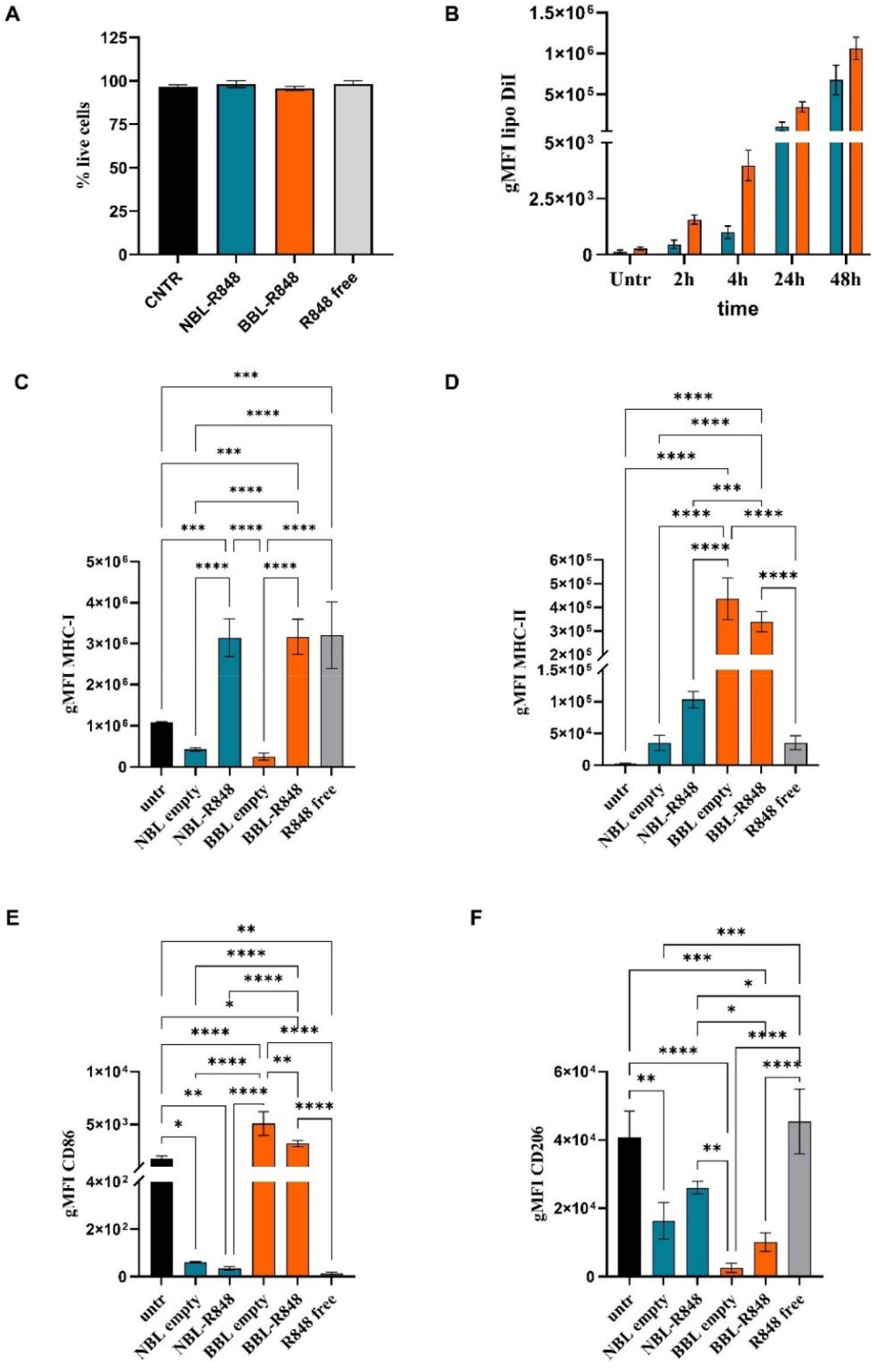

Figure 5. Flow cytometry analyses of primary BMDM (A) viability, (B) in vitro internalization kinetics of fluorescent liposomes expressed as (B) the variation of geometric mean fluorescence intensity (gMFI). (C-F) variation of surface markers expression on M0 macrophages exposed to free R848, or R848-loaded NBL/BBL, (all 1 µM equivalent to free drug) for 48h (n = 3 independent experiments). Statistically significant differences are expressed as follows: *p < 0.05; **p < 0.01; ***p < 0.0001; ****p < 0.00001. Statistically significant differences are listed in Supplementary File 1.

uptake occurs over time, reaching maximum levels at 48h, for both formulations; these data also suggested the ideal time point for observing phenotypical and transcriptional changes due to internalization.

Then, BMDM were treated with NBL or BBL, loaded or not, and after 48h harvested and stained for flow cytometry analysis of inflammatory marker MHC-I (Figure 5(C)), MHC-II (Figure 5(D)), and CD86 (Figure 5(E)) or M2 marker CD206 (Figure 5(F)). Both drug-loaded NBL and BBL induced a statistically significant increase of MHC-I, MHC-II and a reduction of the CD206 compared to untreated samples. Notably, BBL both empty and drug-loaded, demonstrated a higher capacity than drug-loaded NBL-to induce CD86 expression, which was dimly triggered by the free drug. Furthermore, encapsulating an immunostimulant, such as R848, in BBL seems to induce M1 phenotype more efficiently, since CD206 was strongly downregulated by the drug loaded in that formulation compared to NBL or free drug.

Overall, this indicates that the formulations are internalized by 48h, the time at which the drug induces a shift of M0 toward the M1 phenotype; BBL seem to be more efficient in inducing this phenotypic change, thus providing an advantage when using immunostimulants.

NBL and BBL properly release the encapsulated drug maintaining its properties

To explore the ability of each liposome formulation in releasing the drug, not interfering with the immunostimulatory properties of the drug, we used NBL and BBL upon primary BMDMs. Firstly, cells were generated from murine bone marrow, and some wells were left naïve M0 or, instead, differentiated *in vitro* toward M1 or M2 phenotype. BMDM M0 and M2 were exposed for 48h to 1 µM equivalent R848-loaded NBL or BBL or free drug, while M1 cells left untreated for being an internal positive reference. After 48h, cells were harvested, media were stored for further analysis, and pellets were used for RNA isolation. Probes for M1 signature genes, like *Nos2, Il12b,* and *Il6,* were used to monitor whether the R848-loaded NBL or BBL induced a pro-inflammatory M1-like phenotype in differentiated M0 and M2 cells, compared to the untreated M0, M1, and M2. As shown in the charts, standard deviations were high in some cases, which is common when using murine primary cells derived from syngeneic mice for *in vitro* assays; in fact, variability can still arise due to intrinsic biological differences between animals, such subtle immunological states, which may impact on the consistency and strength of the observed responses.

We witnessed that empty liposomes formulation did not significantly trigger the expression of those genes. We observed that both R848-loaded formulations, likewise the free R848, strongly induced *Nos2* expression in M0 and M2 cells, reaching the same level of M1 cells. In detail, M2 cells treated with R848-NBL significantly expressed this gene compared to the respective untreated M2 control; the same significance was observed when M0 cells were treated with R848-BBL compared to untreated M0 control (Figure 6(A)).

The *Il12b* gene was induced by R848-NBL on M0 and M2 cells, while R848-BBL triggered its expression on M0 and modestly on M2 cells but still lacking statistical significance (Figure 6(B)).

The *Il6* gene was significantly induced by R848-NBL on M2 cells (compared to untreated M0 and M2 cells), followed by the R848-BBL but without significance (Figure 6(C)).

Overall, both liposome formulations efficiently activate M0 macrophages and reprogram M2 toward an M1-like phenotype, although NBL-R848 exert stronger effects than BBL-R848 and the free drug at transcription level of the investigated pro-inflammatory genes. These results prove that the drug was correctly released intracellularly, and its chemical properties were not altered, inducing the downstream pathways in macrophages.

Cytokines and chemokines secretion induced by NBL and BBL

Supernatants from untreated and treated BMDMs were used to perform cytokines and chemokines secretion and check whether drug-loaded NBL and BBL induce the secretion of pro-inflammatory factors at different rates.

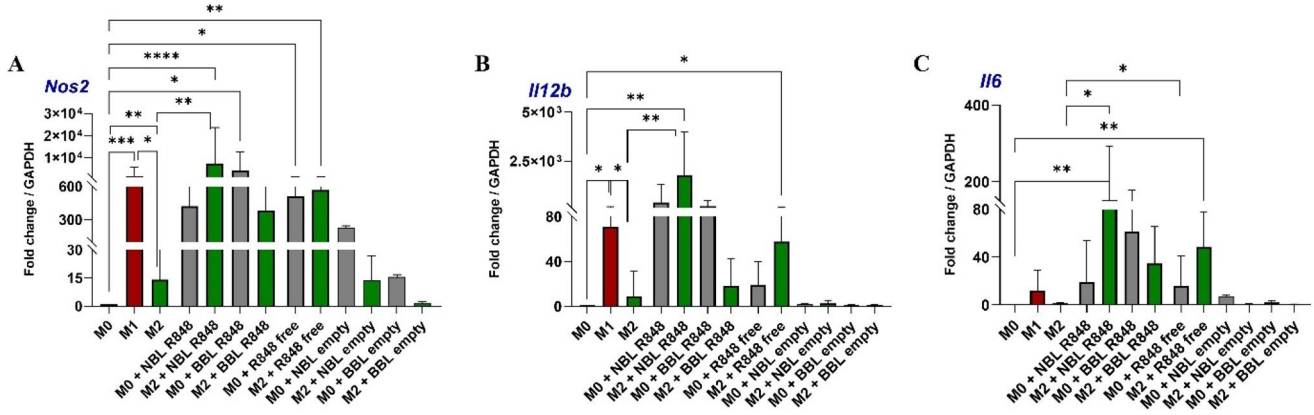

Figure 6. Gene expression analysis on naïve (M0, grey), pro-inflammatory (M1, red), and immunosuppressive (M2, green) BMDMs. M1 signature genes Nos2, Il12b, and Il6 were checked to compare the R848-loaded NBL and BBL (1 µM R848 equivalent) efficacy to induce an inflammatory phenotype at 48h after treatment (n = 6–8 independent experiments with three technical replicates). Results are presented as fold change to the control determined by the ddCt method, using gapdh as a reference gene and unstimulated untreated sample as a calibrator. Statistically significant differences compared to M0, M1, and M2 controls are expressed as follows: *$p < 0.05$; **$p < 0.01$; ***$p < 0.0001$; ****$p < 0.00001$. Statistically significant differences are listed in Supplementary File 1.

As expected, empty NBL and BBL did not induce cytokines or chemokines release significantly compared to controls, meaning that the observed effects were only due to the loaded drug.

Pro-inflammatory cytokines such as interleukin-(IL) 1β, IL-6, and tumor necrosis factor (TNF)-α are endogenous pyrogens produced by activated macrophages that induce a fast response against an infectious agent [39]; their secretion is triggered by both R848-NBL and R848-BBL on M0 and M2 macrophages at levels that overcome the basal secretion of M1 reference cells. This indicates that the R848 drug is released by both liposomal formulations, with NBL showing a statistically significant increase. Another pro-inflammatory cytokine, the IL-12p40 plays a central role in bridging innate and adaptive immunity. The prototypical IL-12 (made by p35/p40 heterodimer), promotes T cells differentiation toward Th1 phenotype, enhances IFN-γ production, and supports cytotoxic T lymphocyte and Natural Killer (NK) cell activation, thereby would drive cellular immune responses against intracellular pathogens and tumors [40]. This molecule is equally and significantly secreted after R848-NBL or R848-BBL exposure, compared to M0 and M2 controls (Figure 7(C)).

Anti-inflammatory cytokines such as transforming growth factor-beta (TGF-β) and IL-10 are key immunoregulatory mediators that help maintain immune homeostasis and prevent

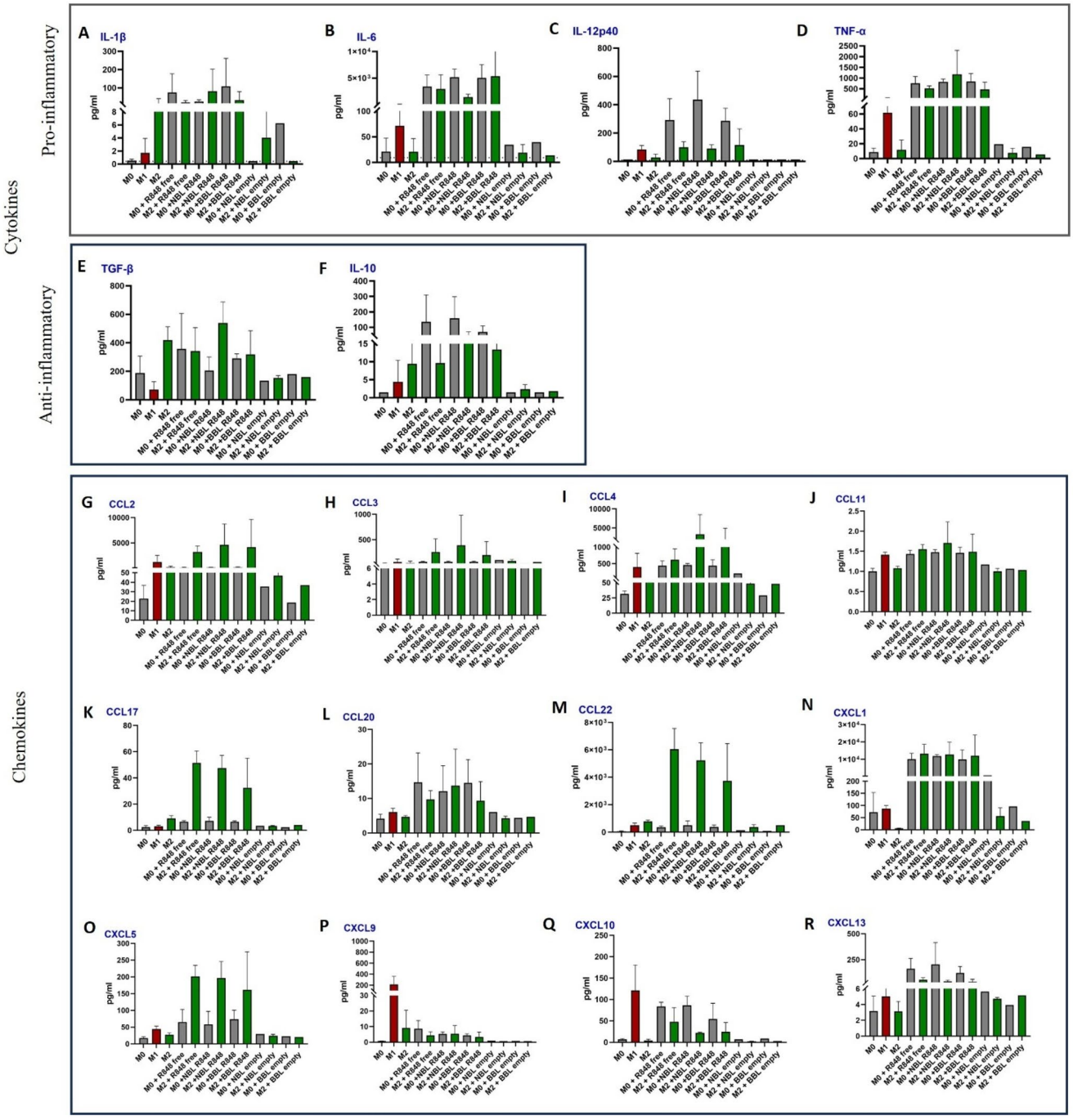

Figure 7. Quantification of the secreted cytokines and chemokines by M0 (grey), M1 (red), and M2 (green) BMDMs. Supernatants were collected from wells after 48h of treatment. Cells were harvested and pelleted, and media were used for quantification of secreted factors by LEGENDPlex assay (n = 4). Statistically significant differences are listed in Supplementary File 1.

excessive inflammation [41]; R848, a synthetic TLR7/8 agonist, induces the production of the anti-inflammatory cytokines IL-10 and TGF-β in macrophages as part of a negative feedback loop to suppress excessive inflammation [42–44].

Drug-loaded NBL significantly induced TGF-β in M2 cells, when compared to M0; instead, IL-10 was induced but not significantly compared to controls (Figure 7(E–F)). Their release does not impede the M1-like phenotype considering the extent of the release of the other pro-inflammatory cytokines.

Chemokines are known to facilitate the process of both migration and infiltration of several effector cells to sites of infection or inflammation while coordinating interactions between those cells [45,46]. By doing so, chemokines link the innate and adaptive immune systems, thus shaping and providing the necessary context for the development of optimal adaptive immune responses [45,46].

We decided to investigate twelve chemokines produced by activated or M1 macrophages to study any possible changes induced by free drug and all liposome formulations.

CCL2, CCL3, and CCL4 are generally involved in modulating T cells and DCs interactions, monocyte trafficking and NK migration [39,45,47]; both R848-NBL and R848-BBL induced their secretion although not significantly (Figure 7(G–I)). CCL11, that promotes eosinophils and basophils migration [45,47], was significantly released by M2 cells after R848-NBL and R848-BBL treatments compared to M0 control (Figure 7(J)). CCL17 and CCL22, involved in Th2 and Treg cells migration [45], were significantly induced by both loaded formulations, compared to M0 and M2 controls (Figure 7(K,M)).

CCL20, which regulates B and Th17 cells responses, was induced by drug-loaded formulations but lacking significance (Figure 7(L)). CXCL1 and CXCL5, that orchestrate monocytes and neutrophils trafficking [45,47], were significantly induced in M2 cells by both loaded formulation, compared to M0 and M2 controls (Figure 7(N,O)). CXCL9 and CXCL10, that regulate Th1 responses, Th1, CD8 and NK trafficking [45,47] were not particularly influenced by the loaded formulations and marginally by the free drug (Figure 7(P,Q)). CXCL13 is a homeostatic B-cells chemoattractant chemokine [45,47] that was significantly released mainly by M0 treated with drug-loaded NBL (Figure 7(R)).

In conclusion, these findings demonstrate that both NBL and BBL formulations effectively release the drug, activating downstream signaling pathways and promoting the secretion of cytokines and chemokines crucial for leukocyte recruitment and activation.

Conclusion

Bone diseases and bone-associated cancers remain difficult to treat due to the lack of targeted and effective therapies. To address this, the study developed bone-targeting liposomes functionalized with a pyrophosphate group (BBL) and compared them to conventional liposomes (NBL). Both formulations showed favorable physicochemical properties and efficient drug encapsulation, with BBL displaying enhanced affinity for the bone matrix. Importantly, neither system was cytotoxic, and both were effectively internalized by macrophages. When loaded with the immunostimulant R848, both liposome types reprogrammed macrophages toward a pro-inflammatory M1-like phenotype, a key step in reversing the immunosuppressive TME.

These findings underscore the therapeutic potential of pyrophosphate-functionalized liposomes for delivering therapeutics directly to bone tissue, where they could improve treatment outcomes in bone diseases and cancers. Future directions include optimization of therapeutic payloads, and exploration of combinatorial strategies with current chemotherapies or immunotherapies to enhance efficacy while minimizing systemic toxicity.

Materials and methods

PPi-PEG3-cholesterol synthesis

PPi-PEG3-cholesterol was prepared through multi-step chemical synthesis (Figure 8) [48]. The connection of the PEG spacer was performed by a preliminary transformation of cholesterol in the corresponding tosylate (1), followed by its substitution with triethylene glycol. The 1° alcohol of ether 2 was also converted into the corresponding tosylate (3). Intermediates 1–3 were all purified by flash chromatography,

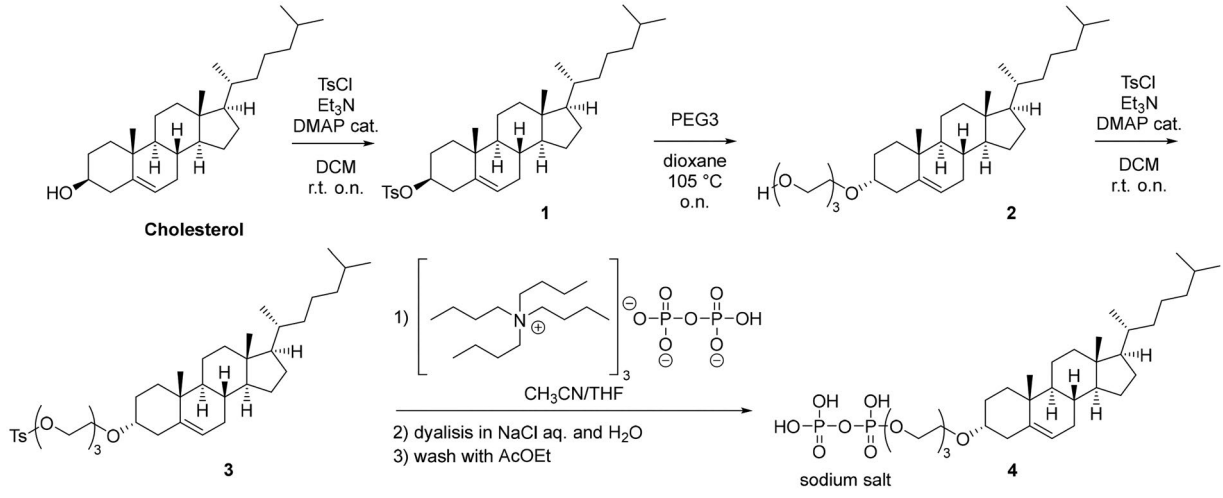

Figure 8. Multi-step chemical synthesis of pyrophosphate-PEG-cholesterol adduct.

where silica gel was used as stationary phase and mixtures of Hex:AcOEt as mobile phase. Product-containing fractions were identified analytical thin-layer chromatography (TLC) using silica gel 60 F254 pre-coated glass plates (0.25 mm thickness).

TLC visualization was accomplished by irradiation with a UV lamp and/or staining with a Ceric Ammonium Molybdate Solution. Finally, tosylate 3 was reacted with the commercially available tetrabutylammonium phosphate salt (Merck). This reaction led to the pyrophosphate-monoester 4. Given the amphiphilic properties of the latter, the crude mixture was dissolved in water and dialyzed (MWCO = 10 kDa) first in a NaCl solution and then water. The solution was further washed with AcOEt to remove the remaining lipophilic material.

Liposome synthesis, characterization

NBL were composed by 1,2-distearoyl-sn-glycero-3-phosphocholine (DSPC, 850365P Avanti Research™, CAS 816–94-4), cholesterol (C8667, Sigma Aldrich, CAS 57–88-5) (70/30 mole ratio); while BBL liposomes were composed by the same DSPC, and cholesterol, and the addition of PPi-PEG3-Cholesterol (70/20/10 mole ratio). Finally, A thin lipid film of 12,5 mg of total lipids was hydrated with 2 ml of 250 mM ammonium sulfate at 58 °C, followed by extrusion with the mini Extruder (Avanti Research™); more than 10 times passage was done using polycarbonate filters of 200 and 100 nm. The liposomes were then dialyzed against an acetate buffer (100 mM, pH 5) to create a transmembrane gradient of ammonium sulfate. R848 was actively loaded into liposomes using ammonium sulfate as a trapping agent [49]. The DLS measurements were performed on dispersions in dH_2O (pH 7) using a Delsa™ Nano Submicron Particle Size and Zeta Potential (Beckmann Coulter) or a Zetasizer Ultra equipped with Multi-Angle Dynamic Light Scattering (MALDLS) technology from Malvern Panalytical and using the software ZS Xplorer.

For the internalization kinetic experiment, liposomes were stained with the lipophilic tracer 1,1′-Dioctadecyl-3,3,3′,3′-Tetramethylindocarbocyanine Perchlorate (DiI, ThermoFisher) after the synthesis and loading procedure. DiI emits at 565 nm, and fluorescence was detected by Cytoflex LX (Beckmann Coulter).

R848 loading and release test

R848 was purchased by MedChem (cat. HY-13740), with a purity of 99.87% by HPLC. The R848 liposomal loading efficiency was evaluated immediately after the production of each BBL and NBL batch via HPLC analysis. The BBL and NBL release profiles were investigated in triplicate by loading 2 ml of each formulation at the R848 concentration of 0.2 mg/ml in the dialysis cassette (Slide-A-Lyzer™, molecular weight cut-off 3.5 kDa, Thermo Fisher Scientific Inc.) and immersed in 200 ml of PBS added with 40 g/L of albumin. Aliquots of 0.1 ml were taken from the dialysis cassette solution at predetermined time points (0.08, 0.25, 0.5, 1, 2, 4 h). The R848 loading amount was determined by HPLC-UV at 230 nm. Briefly, 0.05 ml of liposome solution was spiked with 3 µg of IS and extracted with 0.5 ml of chloroform:isopropanol, (1:1, v/v). After vortexing for 10 s, the samples were centrifuged at 13 000 rpm for 10 min. The organic phase was separated and dried under nitrogen, and the residues were dissolved with 100 µl of H_2O:CH_3CN, 0.1%HCOOH (85:15, v/v). Then 50 µL of the reconstitute samples were injected in the HPLC- UV system ARC (Waters, Milford, Massachusetts, USA). Empty liposome samples were used to prepare the calibration curve with the addition of R848 at different concentrations.

Bone marrow derived macrophages generation and treatments

In vitro differentiated bone marrow-derived primary macrophages were obtained by extracting the whole bone marrow from Balb/c mice bones; precursors were plated in complete medium (RPMI 1640, Euroclone) + 10% FBS (Hyclone, Logan, UT) with macrophage colony-stimulating factor (M-CSF) (25 ng/ml, Peprotech, ThermoFisher) for 5 days. In some cases, macrophages were stimulated with lipopolysaccharide (100 ng/mL; L4524, Sigma Aldrich, Merck), and IFN-g (20 ng/mL; Peprotech, ThermoFisher) for getting M1, or IL-4 (20 ng/mL; Peprotech, ThermoFisher) for M2 phenotype. After 24h, the stimulating media was replenished with new media before each treatment.

Internalization kinetics and markers expression by flow cytometry

After being generated, BMDM were seeded in 24 well-plates with a density of 300.000/well. The day after, assuring the adhesion to the plates, cells were used for the viability and phenotyping assay. Cells were harvested and centrifuged to remove the media. Pellets were resuspended in PBS for the live/dead staining using Viakrome808 (Beckman Coulter), for 15 min in the dark. Then cells were stained for extracellular markers using a PBS−/− buffer containing 2% FBS, 2 mM EDTA and 0.05% NaN3 for 40 min at 4 °C. The anti-murine mAbs mix (all Biolegend): CD45 (clone 30-F11), CD11c (clone N418), CD11b (clone M1/70), F4/80 (clone BM8), MHC-I (H-2Kd-2Dd) (clone 34–1-2S), MHC II (I-A,I-E) (clone M5/114.15.2), CD86 (clone GL1), CD206 (clone C068C2), all used at specific dilutions, based on previous titration.

Samples acquisition (30.000 events) was performed by Cytoflex LX (Beckmann Coulter). Data analysis was performed by FlowJov10 Software (BD LifeSciences).

RNA isolation and qRT-PCRs

Total RNA was isolated using RNeasy Mini Kit (Qiagen), and cDNA was transcribed using the High-Capacity cDNA Reverse Transcription Kit. A quantitative polymerase chain reaction (qPCR) was performed using the TaqMan assay from ThermoFisher Scientific following the manufacturer's instructions, and the samples were analyzed on 7900HT Fast Real-Time PCR System with 384-Well Block Module. For each gene, mRNA was normalized to *Gapdh* mRNA by subtracting the cycle threshold (Ct) value of *Gapdh* mRNA from the Ct value of the gene (ΔCt). The fold difference ($2^{-\Delta\Delta Ct}$) was calculated by comparing the ΔCt with the ΔCt of unstimulated cells [50]. Three technical replicates were set for each condition.

Liposomes internalization inhibition

After being generated, BMDM were seeded in 24 well-plates with a density of 150.000/well. The day after, assuring the adhesion to the plates, cells were treated for 30 min with the inhibitors at the following concentration: 25 uM Pitstop2 (SML1169), 0,5 µg/mL Filipin III from *Streptomyces filipinens* (F4767), 10 µg/mL 5-(N-ethyl-N-isopropyl)-amiloride (EIPA) (A3085) (all Sigma-Aldrich). Afterwards, NBL or BBL were added to the culture and harvested after 1, 2, 4, 6, 8, 24h and acquired at the Cytoflex LX (Beckmann Coulter). Data analysis was performed by FlowJov10 Software (BD LifeSciences).

Chemokines and cytokines quantification by flow cytometry

Cell culture supernatants were collected and stored at −80 °C until needed. On the day of the analysis, supernatants were thawed and used for running the Biolegend LEGENDplex™ assays: Mouse Macrophage/Microglia Panel (13-plex) and Mouse Proinflammatory Chemokine (13-plex) following the manufacturer's instructions. Samples were acquired at the Cytoflex LX (Beckmann Coulter), and data analysis was performed using the Biolegend online platform.

Animals

Nine-to-12-week-old female Balb/C mice were obtained from Charles River Laboratories (Calco, Italy). They were maintained under specific pathogen-free conditions, housed in isolated vented cages, and handled using aseptic procedures after an acclimatization period of one week. Mice were regularly checked by a certified veterinarian, who was responsible for health monitoring, animal welfare supervision, experimental protocols and review of procedures. Procedures involving animals and their care were conducted in conformity with the institutional guidelines that comply with the Italian Governing Law (D.lgs 26/2014), with the Mario Negri Institutional regulations and policies that provide internal authorization for people conducting animal experiments (Quality Management System Certificate – UNI EN ISO 9001:2015 – Reg. No. 6121) and with the National Institutes of Health (NIH) Guide for the Care and Use of Laboratory Animals (2011 edition) and EU directives and guidelines (EEC Council Directive 2010/63/UE). The Italian Ministry of Health (authorization no. 9F5F5.N.IXK) approved the use of animals for this study.

Samples preparation for confocal microscopy

Bones were sampled postmortem from healthy mice and used for a qualitative assay. Femurs were incubated at 37 °C for 2h or 24h with R848-loaded NBL or BBL equivalent doses of 1 µM of R848. Afterward, bones were washed 10 times with PBS before image acquisition to remove any unbound liposomes.

Images were acquired using sequential scanning mode by an A1 Nikon confocal running NIS Elements at 20X or 40X magnification. Data was acquired using NIS Elements software 4.5 (Nikon, Melville, NY, USA).

Statistical analysis

All the data are indicated as mean ± SD. When stated, independent experiment means a single experiment carried out with a new liposome batch and with a new batch of primary macrophages. Statistical analysis and the significant differences among the means were analyzed by one way analysis of variance (ANOVA) test with Dunnet correction: non-parametric for data of Figure 5, and parametric for all the other data (GraphPad v10.4 Software). Statistically significant differences were expressed as follows: $*p < 0.05$; $**p < 0.01$; $***p < 0.0001$; $****p < 0.00001$.

Authors contribution

CN: conceptualization, original draft preparation, writing, data analysis, and fundings. ADC, RB: chemical synthesis. CN, RB, ST: *in vitro* experiment, flow-cytometry. CM, MC, MM, GG: HPLC and analysis. GN, RF, MZ: data analysis and interpretation. PF: confocal microscopy. All authors: data discussion and manuscript corrections. All authors have read and edited the manuscript and agreed to the published version.

Disclosure statement

No potential conflict of interest was reported by the author(s).

Funding

Fondazione Beppe and Nuccy Angiolini Onlus supported this research.

References

[1] Song S, Guo Y, Yang Y, et al. Advances in pathogenesis and therapeutic strategies for osteoporosis. Pharmacol Ther. 2022;237:108168. doi:10.1016/j.pharmthera.2022.108168.
[2] Clarke B. Normal bone anatomy and physiology. Clin J Am Soc Nephrol. 2008;3(Suppl 3):S131–S139. doi:10.2215/CJN.04151206.
[3] Mallorie A, Shine B. Normal bone physiology, remodelling and its hormonal regulation. Surgery (Oxford). 2022;40(3):163–168. doi:10.1016/j.mpsur.2021.12.001.
[4] Wu Y, Sun B, Tang Y, et al. Bone targeted nano-drug and nano-delivery. Bone Res. 2024;12(1):51. doi:10.1038/s41413-024-00356-2.
[5] Morya VK, Magar AG, Park S-H, et al. Systemic strategies for osteosarcoma: advances and future directions. Discov Oncol. 2025;16(1):1367. doi:10.1007/s12672-025-02208-9.
[6] Strauss SJ, Berlanga P, McCabe MG. Emerging therapies in ewing sarcoma. Curr Opin Oncol. 2024;36(4):297–304. doi:10.1097/CCO.0000000000001048.
[7] Choi JH, Ro JY. The 2020 WHO classification of tumors of bone: an updated review. Adv Anat Pathol. 2021;28(3):119–138. doi:10.1097/PAP.0000000000000293.
[8] Coleman R, Hadji P, Body J-J, et al. Bone health in cancer: ESMO clinical practice guidelines. †Ann Oncol. 2020;31(12):1650–1663. doi:10.1016/j.annonc.2020.07.019.
[9] Coleman RE, Brown J, Holen I. 56 - Bone metastases. In Abeloff's clinical oncology. (Sixth Edition) Niederhuber, J. E., Armitage, J. O., Kastan, M. B., Doroshow, J. H. & Tepper, J. E. (eds.) Elsevier: Philadelphia; 2020. 809–830.e3. doi:10.1016/B978-0-323-47674-4.00056-6.
[10] Coleman RE. Metastatic bone disease: clinical features, pathophysiology and treatment strategies. Cancer Treat Rev. 2001;27(3):165–176. doi:10.1053/ctrv.2000.0210.
[11] Coleman RE. Clinical features of metastatic bone disease and risk of skeletal morbidity. Clin Cancer Res. 2006;12(20 Pt 2):6243s–6249s. doi:10.1158/1078-0432.CCR-06-0931.

[12] Xu H, Wang W, Liu X, et al. Targeting strategies for bone diseases: signaling pathways and clinical studies. Signal Transduct Target Ther. 2023;8(1):202. doi:10.1038/s41392-023-01467-8.
[13] Wu Y, , et al. Bone targeted nano-drug and nano-delivery. Bone Res. 2024;12.
[14] Gabizon AA. Selective tumor localization and improved therapeutic index of anthracyclines encapsulated in long-circulating liposomes. Cancer Res. 1992;52(4):891–896.
[15] Wang B, Hu S, Teng Y, et al. Current advance of nanotechnology in diagnosis and treatment for malignant tumors. Sig Transduct Target Ther. 2024;9(1):1–65. doi:10.1038/s41392-024-01889-y.
[16] Liu P, Chen G, Zhang J. A review of liposomes as a drug delivery system: Current status of approved products, regulatory environments, and future perspectives. Molecules. 2022;27(4):1372. doi:10.3390/molecules27041372.
[17] Alameh M-G, Tombácz I, Bettini E, et al. Lipid nanoparticles enhance the efficacy of mRNA and protein subunit vaccines by inducing robust T follicular helper cell and humoral responses. Immunity. 2021;54(12):2877–2892.e7. doi:10.1016/j.immuni.2021.11.001.
[18] Andra VVSNL, Pammi SVN, Bhatraju LVKP, et al. A comprehensive review on novel liposomal methodologies, commercial formulations, clinical trials and patents. Bionanoscience. 2022;12(1):274–291. doi:10.1007/s12668-022-00941-x.
[19] Huwyler J, Drewe J, Krähenbuhl S. Tumor targeting using liposomal antineoplastic drugs. Int J Nanomedicine. 2008;3(1):21–29.
[20] O'Brien MER, Wigler N, Inbar M, et al. Reduced cardiotoxicity and comparable efficacy in a phase IIItrial of pegylated liposomal doxorubicin HCl(CAELYX™/doxil®) versus conventional doxorubicin forfirst-line treatment of metastatic breast cancer. Annals Oncol. 2004;15(3):440–449. doi:10.1093/annonc/mdh097.
[21] Gabizon A, Papahadjopoulos D. Liposome formulations with prolonged circulation time in blood and enhanced uptake by tumors. Proc Natl Acad Sci U S A. 1988;85(18):6949–6953. doi:10.1073/pnas.85.18.6949.
[22] Lee JH, Yeo Y. Controlled drug release from pharmaceutical nanocarriers. Chem Eng Sci. 2015;125:75–84. doi:10.1016/j.ces.2014.08.046.
[23] Ferreira M, Ogren M, Dias JNR, et al. Liposomes as antibiotic delivery systems: a promising nanotechnological strategy against antimicrobial resistance. Molecules. 2021;26(7):2047. doi:10.3390/molecules26072047.
[24] Agrawal SS, Baliga V, Londhe VY. Liposomal formulations: a recent update. Pharmaceutics. 2024;17(1):36. doi:10.3390/pharmaceutics17010036.
[25] Kumbham S, Ajjarapu S, Ghosh B, et al. Current trends in the development of liposomes for chemotherapeutic drug delivery. J Drug Delivery Sci Technol. 2023;87:104854. doi:10.1016/j.jddst.2023.104854.
[26] Gordon AN, Fleagle JT, Guthrie D, et al. Recurrent epithelial ovarian carcinoma: a randomized phase III study of pegylated liposomal doxorubicin versus topotecan. J Clin Oncol. 2001;19(14):3312–3322. doi:10.1200/JCO.2001.19.14.3312.
[27] Halford S, Yip D, Karapetis CS, et al. A phase II study evaluating the tolerability and efficacy of CAELYX (liposomal doxorubicin, doxil) in the treatment of unresectable pancreatic carcinoma. Ann Oncol. 2001;12(10):1399–1402. doi:10.1023/a:1012522120294.
[28] Thomas AL, O'Byrne K, Furber L, et al. A phase II study of caelyx, liposomal doxorubicin: lack of activity in patients with advanced gastric cancer. Cancer Chemother Pharmacol. 2001;48(4):266–268. doi:10.1007/s002800100351.
[29] Fidan Y, Muçaj S, Timur SS, et al. Recent advances in liposome-based targeted cancer therapy. J Liposome Res. 2024;34(2):316–334. doi:10.1080/08982104.2023.2268710.
[30] Burduşel A-C, Andronescu E. Lipid nanoparticles and liposomes for bone diseases treatment. Biomedicines. 2022;10(12):3158. doi:10.3390/biomedicines10123158.
[31] Cremers S, Drake MT, Ebetino FH, et al. Pharmacology of bisphosphonates. Br J Clin Pharmacol. 2019;85(6):1052–1062. doi:10.1111/bcp.13867.
[32] Hemmi H, Kaisho T, Takeuchi O, et al. Small anti-viral compounds activate immune cells via the TLR7 MyD88–dependent signaling pathway. Nat Immunol. 2002;3(2):196–200. doi:10.1038/ni758.
[33] Jurk M, Heil F, Vollmer J, et al. Human TLR7 or TLR8 independently confer responsiveness to the antiviral compound R-848. Nat Immunol. 2002;3(6):499–499. doi:10.1038/ni0602-499.
[34] Michaelis KA, Norgard MA, Zhu X, et al. The TLR7/8 agonist R848 remodels tumor and host responses to promote survival in pancreatic cancer. Nat Commun. 2019;10(1):4682. doi:10.1038/s41467-019-13151-z.
[35] Rodell CB, Arlauckas SP, Cuccarese MF, et al. TLR7/8-agonist-loaded nanoparticles promote the polarization of tumour-associated macrophages to enhance cancer immunotherapy. Nat Biomed Eng. 2018;2(8):578–588. doi:10.1038/s41551-018-0236-8.
[36] Russo M, Nastasi C. Targeting the tumor microenvironment: a close up of tumor-associated macrophages and neutrophils. Front Oncol. 2022;12:871513. doi:10.3389/fonc.2022.871513.
[37] Dutta D, Donaldson JG. Search for inhibitors of endocytosis: Intended specificity and unintended consequences. Cell Logist. 2012;2(4):203–208. doi:10.4161/cl.23967.
[38] Gandek TB, van der Koog L, Nagelkerke A. A comparison of cellular uptake mechanisms, delivery efficacy, and intracellular fate between liposomes and extracellular vesicles. Adv Healthc Mater. 2023;12(25):e2300319. doi:10.1002/adhm.202300319.
[39] Murphy K, Weaver C. Janeway's immunobiology. (New York and London: Garland Science, Taylor & Francis Group, LLC, 2017).
[40] Trinchieri G. Interleukin-12 and the regulation of innate resistance and adaptive immunity. Nat Rev Immunol. 2003;3(2):133–146. doi:10.1038/nri1001.
[41] Li MO, Flavell RA. TGF-β: a master of all T cell trades. Cell. 2008;134(3):392–404. doi:10.1016/j.cell.2008.07.025.
[42] Levy O, Zarember KA, Roy RM, et al. Selective impairment of TLR-mediated innate immunity in human newborns: neonatal blood plasma reduces monocyte TNF-alpha induction by bacterial lipopeptides, lipopolysaccharide, and imiquimod, but preserves the response to R-848. J Immunol. 2004;173(7):4627–4634. doi:10.4049/jimmunol.173.7.4627.
[43] Lombardi V, Van Overtvelt L, Horiot S, et al. Human dendritic cells stimulated via TLR7 and/or TLR8 induce the sequential production of Il-10, IFN-gamma, and IL-17A by naive CD4+ T cells. J Immunol. 2009;182(6):3372–3379. doi:10.4049/jimmunol.0801969.
[44] Nahid MA, Benso LM, Shin JD, et al. TLR4, TLR7/8 agonist-induced miR-146a promotes macrophage tolerance to MyD88-dependent TLR agonists. J Leukoc Biol. 2016;100(2):339–349. doi:10.1189/jlb.2A0515-197R.
[45] Sokol CL, Luster AD. The chemokine system in innate immunity. Cold Spring Harb Perspect Biol. 2015;7(5):a016303. doi:10.1101/cshperspect.a016303.
[46] Ozga AJ, Chow MT, Luster AD. Chemokines and the immune response to cancer. Immunity. 2021;54(5):859–874. doi:10.1016/j.immuni.2021.01.012.
[47] Hughes CE, Nibbs RJB. A guide to chemokines and their receptors. Febs J. 2018;285(16):2944–2971. doi:10.1111/febs.14466.
[48] Liu Y, Jia Z, Ma L, et al. Pyrophosphorylated-Cholesterol-modified bone-targeting liposome formulation procedure. in Liposomes: Methods and protocols. (eds. D'Souza, G. G. M. & Zhang, H.) 207–220. Springer US, New York, NY, 2023). doi:10.1007/978-1-0716-2954-3_18.
[49] Pauli G, Chao P-H, Qin Z, et al. Liposomal resiquimod for enhanced immunotherapy of peritoneal metastases of colorectal cancer. Pharmaceutics. 2021;13(10):1696. doi:10.3390/pharmaceutics13101696.
[50] Livak KJ, Schmittgen TD. Analysis of relative gene expression data using Real-Time quantitative PCR and the $2-\Delta\Delta CT$ method. Methods. 2001;25(4):402–408. doi:10.1006/meth.2001.1262.